3D studies of indentation by combined X-ray tomography and digital volume correlation

Mahmoud Mostafavi[1,#], Yelena Vertyagina[1], Christina Reinhard[2], Robert Bradley[3], Xia Jiang[1], Marina Galano[1] and James Marrow[1,#]

[1] Department of Materials and [#]Oxford Martin School, University of Oxford, UK

[2] Diamond Light Source, Harwell Science and Innovation Campus, Oxfordshire, UK

[3] Manchester X-ray Imaging Centre, University of Manchester, UK

james.marrow@materials.ox.ac.uk

Keywords: Computed Tomography, Hardness, Indentation, Digital Image Correlation

Abstract Hardness testing obtains material properties from small specimens via measurement of load-displacement response to an imposed indentation; it is a surface characterisation technique so, except in optically transparent materials, there is no direct observation of the assumed damage and deformation processes within the material. Three-dimensional digital image correlation ('digital volume correlation') is applied to study deformation *beneath* indentations, mapping the relative displacements between high-resolution synchrotron X-ray computed tomographs (0.9 μm voxel size). Two classes of material are examined: ductile aluminium-silicon carbide composite (Al-SiC) and brittle alumina (Al_2O_3). The measured displacements for Hertzian indentation in Al-SiC are in good agreement with an elastic-plastic finite element simulation. In alumina, radial cracking is observed beneath a Vickers indentation and the crack opening displacements are measured, in situ under load, for the first time. Potential applications are discussed of this characterization technique, which does not require resolution of microstructural features.

Introduction

Hardness testing has long been used to interrogate materials to understand their deformation and fracture. The dimensions of an indentation (e.g. projected area and depth, sometimes with surface profile analysis of pile-up/sink-in) are used to infer the processes of deformation that have occurred underneath indenters of various size and shape [1-6]. With appropriate assumptions or understanding of deformation processes, such as strain-hardening in ductile materials, hardness tests on small samples can be used to evaluate the effects of subtle changes in microstructure on the mechanical properties of engineering components (for instance, the effects of fast neutron irradiation and thermal ageing on structural steels in structural nuclear steels [7, 8]). Fracture behaviour can also be studied; there is a range of indentation methods for fracture toughness measurements in brittle materials, although these are complicated by the various types of cracking that develop depending on material properties [9, 10].

Hardness testing is a surface characterisation technique and, except in transparent materials, it provides no direct observation of the assumed damage and deformation processes. Digital image correlation is a highly precise displacement measurement method with many applications [11]; some of the authors have applied it to measure surface deformation in studies of cracking processes [12], for instance. In appropriate microstructures, X-ray tomography can be combined with three-dimensional digital image correlation (digital volume correlation or DVC) [13] to measure the deformation *within* materials [14-16]. Such data may be used to validate models for deformation and fracture behaviour. Sufficient contrast may be achieved from microstructural heterogeneities of

the order of the voxel[1] size. The precision of displacement resolution increases with the multi-voxel interrogation window size, enabling DVC to measure sub-voxel displacements [17].

DVC is applied here to high-resolution synchrotron X-ray computed tomography observations, obtained in situ under load, to study indentation behaviour in two types of materials; aluminium-silicon carbide composite (Al-SiC: 6061 Al alloy reinforced with 15wt% SiC particles of 500 nm average size, extruded at 450 °C) and commercial purity alumina (Al_2O_3). The high brilliance and penetration of synchrotron X-rays, compared to laboratory sources, allows sequential observations of representative volumes of engineering materials [18-20]. The measured displacements in Al-SiC are compared with predictive models for elastic-plastic indentation in a ductile material, whilst in Al_2O_3 the displacement field is used to detect cracking beneath the indentation in a brittle material and to extract the crack opening displacements.

Experiment

The specimens, an Al-SiC cylinder (3 mm in diameter, 4 mm high) and an Al_2O_3 rectangular prism (3 × 3 mm square, 4 mm high), were indented using a 5 mm radius Al_2O_3 ball (i.e. Hertzian) and a 'Vickers' square pyramidal diamond respectively, by a loading stage that had been modified to accommodate the indenters. High resolution computed synchrotron X-ray tomography was performed at the Diamond Light Source, Joint Engineering, Environmental and Processing beamline (I12 – JEEP), using radiographic projections obtained at an X-ray beam energy of 53 keV with a nominal voxel size of 0.9 μm. The exposure time was 2 seconds per radiograph for both materials, with projections at increments of 0.04 degrees over 180° rotation. Reference tomographs were recorded under a small pre-load (nominally 10 N), applied to reduce rigid body movement between successive scans. The maximum applied load on the Al-SiC sample was 500 N (indentation depth 47 μm, measured from radiographs), which dropped to 480 N during the tomography scan, and that on the alumina was 360 N (indentation depth 35 μm), which dropped to 330 N during the tomography scan.

A combined Fourier-wavelet ring artefact removal algorithm [21] was used to suppress ring artefacts in the reconstructed tomographs. These arise from instrument features such as defective pixels in the scintillator; if not adequately supressed they can significantly increase noise in the DVC analysis as they do not displace with the material. Example *xy*-plane slices of the tomographs are shown in Figure 1; these are effectively maps of the differences in X-ray attenuation in the sample due to its microstructure. The fine porosity in the Al_2O_3 is well resolved, but the contrast in the Al-SiC composite is low as both phases have very similar X-ray attenuation: Al (density 2.7 g cm^{-3}) has an attenuation coefficient (including coherent scattering) of 0.334 cm^2 g^{-1} at 53 keV, compared to 0.331 for SiC (density 3.1 g cm^{-3}). The calculated absorption contrast difference is only 13% [22]; this could be enhanced if energies below the absorption edge in SiC around 2 keV were used, but this is not practical. However, there is a degree of phase contrast from microstructure interfaces due to the sample-camera distance and coherent X-rays [23]. Artefacts remain in the tomographs; low contrast bands that are a characteristic of the wavelet algorithm are observed in the Al-SiC composite and radial streaks emerge from the region below the indentation in Al_2O_3. These may be edge artefacts [24], from the strong difference in attenuation between Al_2O_3 and open regions of radial cracks that are aligned with the projection axis of some radiographs. Cracking, expected at the applied indentation load, is not observable in the tomographic image.

[1] A voxel is the three-dimensional equivalent of a pixel.

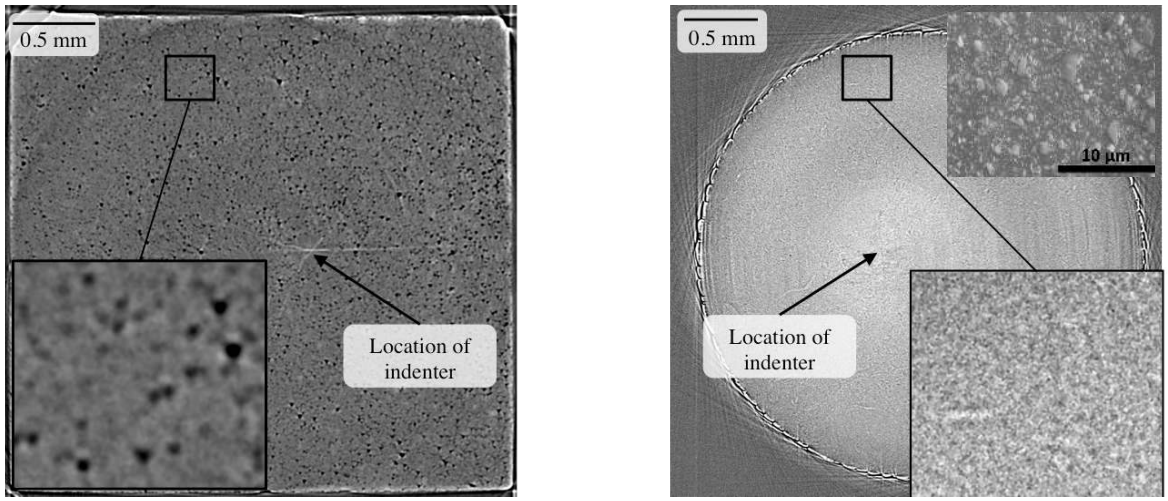

a) b)

Figure 1: Examples of reconstructed tomography slices in the *xy* plane; a) Al_2O_3 and b) Al-SiC composite (inset top right: scanning electron microscope image of Al-SiC microstructure).

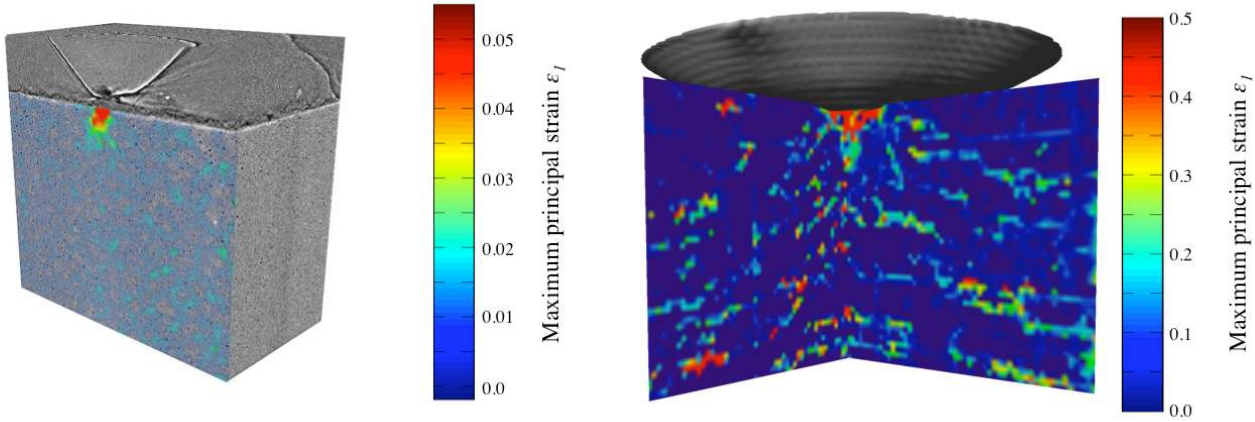

a) b)

Figure 2: Visualisations of maximum principal strain a) Al_2O_3 and b) Al-SiC composite. (the sample field of view is approximately 3 mm in each case)

Analysis

The DVC analyses were carried out using the Davis Strain Master 8.1 software [25], correlating a loaded 3D dataset (i.e. tomograph) against its reference to map the relative displacements. Each dataset measured 4016×4008×2672 voxels (160 GB as 32 bit data), cropped to 3504×3504×2000 voxels and converted to 8 bit data (reduced to 24 GB) for Al-SiC and 2600×2600×2000 voxels (13GB at 8 bit) for Al_2O_3. Vertical (*z*) rigid body movements between datasets were corrected by visual matching of image slices in an *xy* plane close to the indented surface. For Al_2O_3, the following image correlation parameters were judged to be optimal; 256×256×256 voxel interrogation window, 50% overlap and 2 passes, followed by 128×128×128 interrogation window, 75% overlap and 3 passes. For Al-SiC it was necessary to use a 256×256×256 interrogation window, 50% overlap, 2 passes and followed by 64×64×64 interrogation window, 50% overlap and 2 passes. Reducing the final interrogation window size increases the displacement map spatial resolution, though excessive noise arises with smaller window size. Overlapping interrogation windows may improve the displacement map spatial resolution in smoothly changing fields, allowing the use of larger interrogation windows to reduce measurement noise. Increasing the number of passes may also reduce noise, with a diminishing effect with increasing passes. The deformation may be visualised as a nominal strain, obtained from the displacement gradient; examples are given in Figure 2. These show that deformation has occurred under the indentor in the Al-SiC and Al_2O_3, but the images are not very suitable for quantitative analysis.

Examples of the displacement fields in the indented Al-SiC and Al_2O_3 are presented in Figure 3, illustrating the relative vertical displacements (V_z) in the *xy* plane. White patches are regions where displacement vectors were removed due to poor correlation. Due to higher levels of noise in the low contrast Al-SiC data, a relatively stringent criterion was applied, removing displacement vectors with poor correlation (correlation coefficient < 0.6); less stringent filtering was applied to the Al_2O_3. Consequently Figure 3a shows more white patches than Figure 3b. The image artefacts described earlier may be responsible for some regions of poor correlation.

As presented, both datasets are affected by a small rigid body rotation between the reference and loaded tomographs. This dominates the relative displacement field and thus the deformation arising from the indentation is difficult to observe. The DVC analysis software can be used to correct for this by first calculating the relative rotations between tomographs using a large interrogation window, which increases precision and reduces local effects, then adjusting one tomography dataset by interpolation to remove this rotation. Correlation with smaller interrogation windows is then applied to the interpolated dataset. The authors have implemented a more computationally efficient method, based on [26], which considers the relative displacement field from the original tomography data and thus does not require interpolation. Applying this method, the Al-SiC rotated by -0.26°, 0.58° and 3.6° about the *x*, *y* and *z*-axes respectively when loaded (clockwise rotation about the axis is positive), while the Al_2O_3 rotated by -0.54°, -0.33° and 0.34° about the *x*, *y* and *z*-axes respectively. These rotations are attributed to compliance of the loading rig; no evidence was found for flexure of the sample. The corrective rigid body rotation gives a displacement field aligned with the original sample orientation. The vertical displacements below the indentations, after correction for the rigid body rotations, are shown in Figure 4; the effects of the indentations are now well visualised. The compressive strains in the *xz* plane below the indentions, along with the displacement vectors are illustrated in Figure 5. The displacement measurement noise, estimated as the standard error after rotation correction from regions of negligible deformation that are remote from the indentations, was 1.8 µm for the Al-SiC and 0.3 µm for the Al_2O_3.

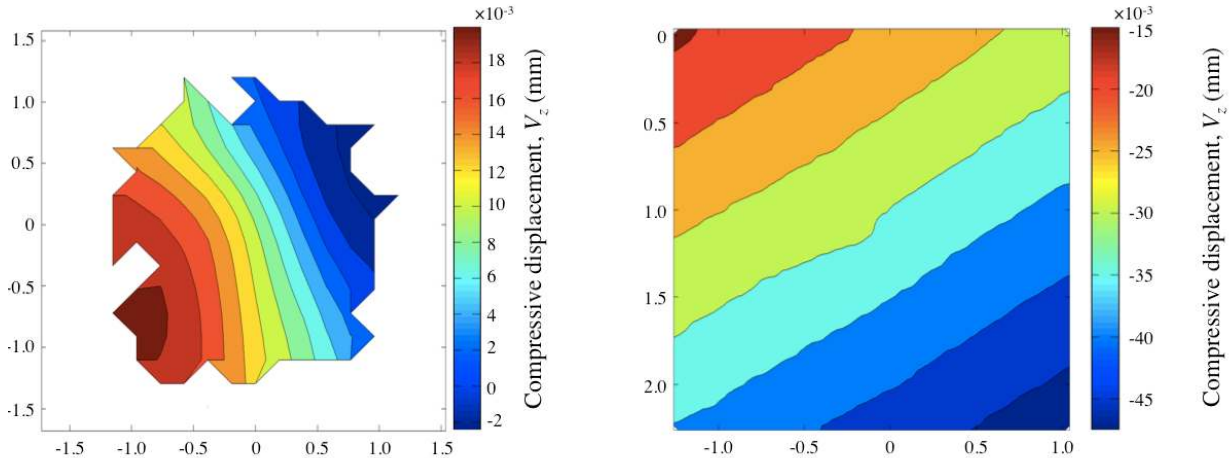

Figure 3: Original vertical (V_z) displacement field in a) Al-SiC in the *xy* plane at 213 voxels (0.192 mm) below the indenter b) Al_2O_3 in the *xy* plane at 96 voxels (0.087 mm) below the indenter.

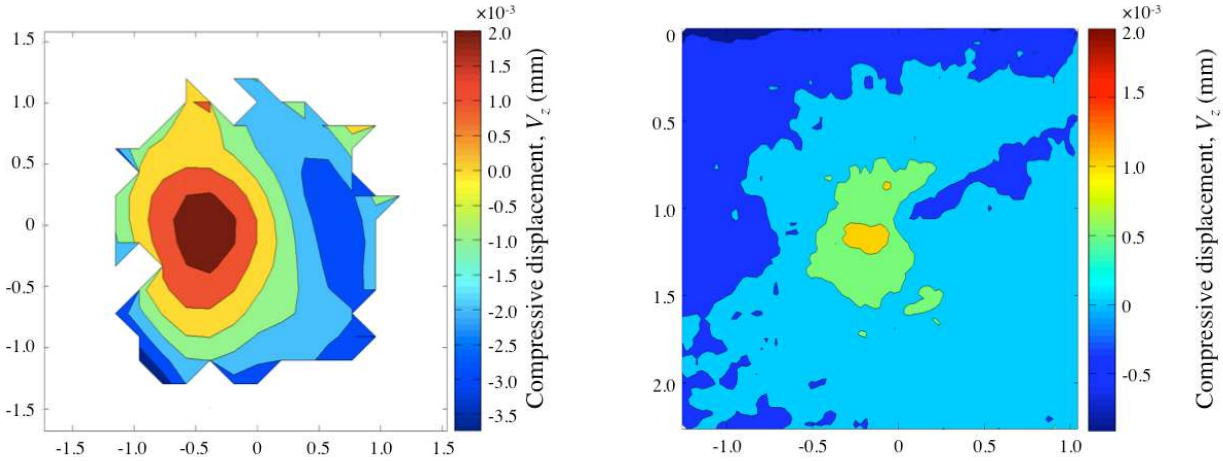

Figure 4: Vertical (V_z) displacement field in *xy* plane below the indenter after rigid body rotation correction in a) Al-SiC at 0.192 mm (213 voxels), b) Al_2O_3 0.087 mm (96 voxels).

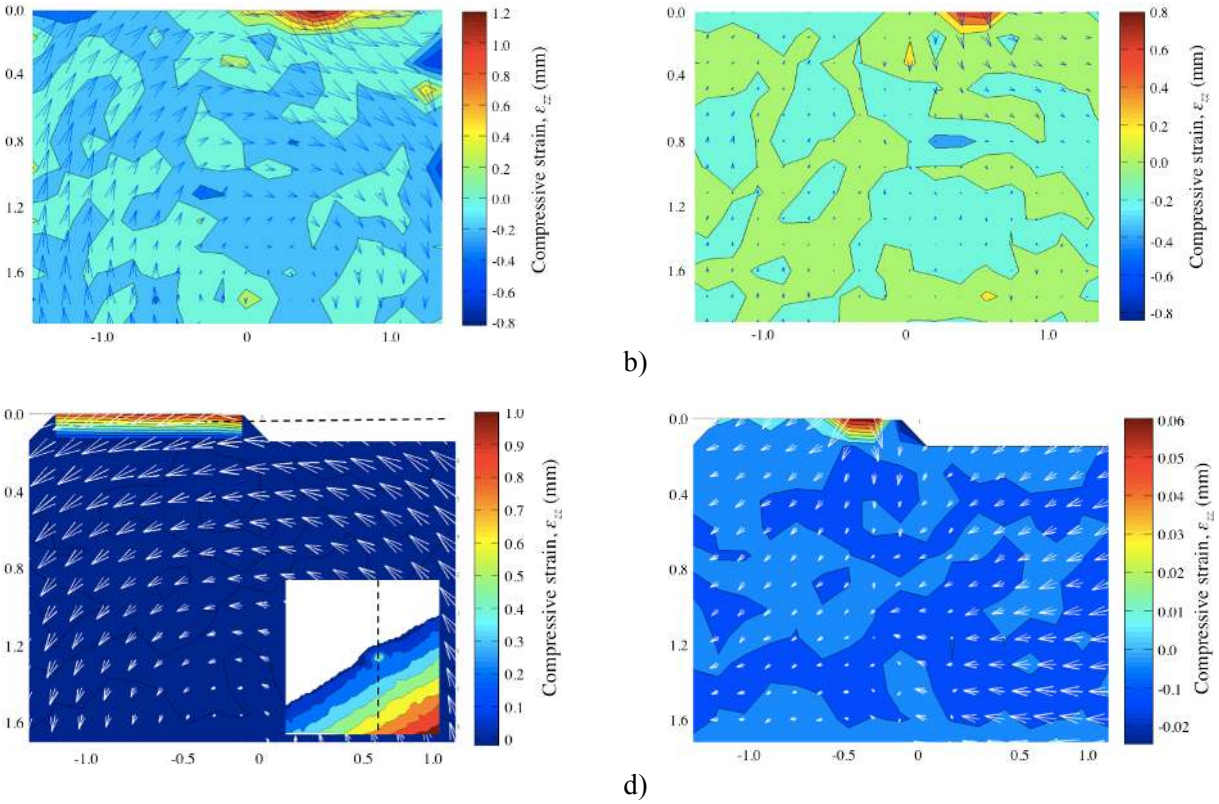

Figure 5: Displacement vectors and compressive strain distribution, ε_{zz}, below the indenter in the *xz* plane at the centre of the indented region. Data before rotation correction (left) and after (right) are compared. Data are shown for Al-SiC (a & b) and Al_2O_3 (c & d). (Every fifth vector is shown, magnified for clarity) – The white patches show the areas where the displacement vectors could not be reliably found. An example of the V_z displacement field in the *xy* plane is inset in c) at the position of the dashed line. Note: z=0 corresponds to the centre of an image correlation window adjacent to the original surface; 64 voxels (58 µm) and 32 voxels (29 µm) below the non-indented surface for Al_2O_3 and Al-SiC respectively.

A 3D finite element simulation of the Hertzian indentation was carried out (ABAQUS v 6.10 [27]), with 1200 rigid elements to simulate the indenter and 18000 solid eight-node brick elements for the Al-SiC. Finite sliding, frictionless contact was modelled and nonlinear elastic (Ramberg-Osgood) material properties defined: elastic modulus 102 GPa; Poisson ratio 0.27; yield stress (0.2% proof stress) 230 MPa and hardening exponent 9. These values were obtained by curve-fitting to tensile data [28], and agree with published results for a similar material [29]. Nonlinear geometry was

used to account for the effect of high levels of deformation on the stiffness matrix. The simulated displacement field depends on the indentation depth and is insensitive to the material properties. The indenter was displaced 47 µm vertically (Figure 6a), obtaining a reaction force of 484 N that agrees well with the experimentally recorded load (480 N). The displacements (V_z) below the indenter also agree with the experimental data (Figure 6b), except close to the surface.

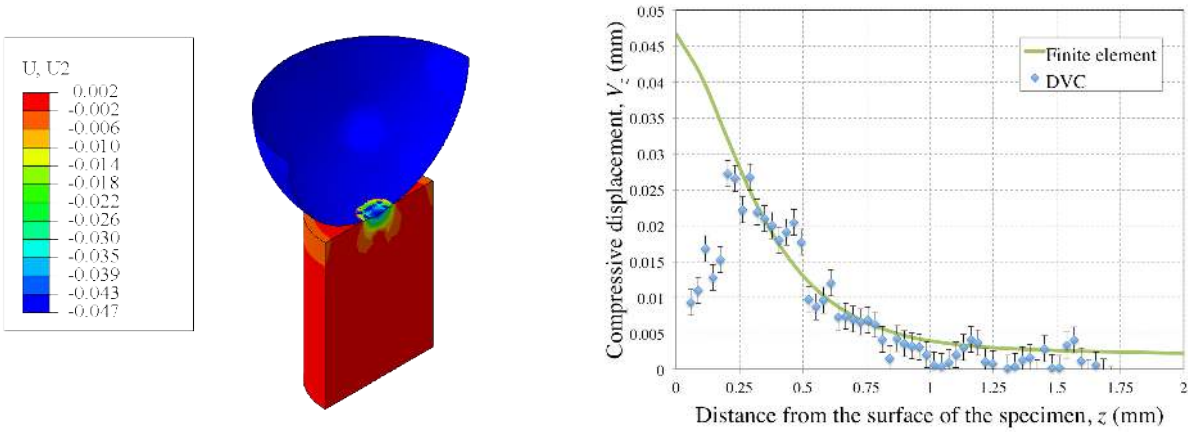

a) b)

Figure 6: Displacements below the Hertzian indentation; a) overview of finite element model showing the vertical displacements (mm), measured relative to the contact between the indenter and sample; b) compressive displacements under the indentation (V_Z) - simulated (FE) and measured (DVC) - the data are individual displacement vectors measured along a vertical line directly below the indenter.

At the applied indentation load, assuming a nominal fracture toughness of 5 MPa $m^{1/2}$ [30], the expected radial crack size in alumina is around 200 µm [9]; but this was not observable in the tomography nor, due to noise, in a visualisation of the displacement gradients as strain. However, a crack may be characterised by measuring the opening displacement across its expected location [12]. Two *xz*-planes were selected from the both sides of the indentation, parallel to a diagonal of the indenter, separated by a distance of 5 displacement vectors (i.e. 0.145 mm in total). To reduce noise, each displacement vector was averaged with the value in the further neighbouring parallel plane (i.e. planes separated by 7 vectors). The relative displacements, δ_x, δ_y, δ_z, were then obtained; data for δ_x and δ_y are shown in Figure 7. The crack opening is given by δ_y; its maximum value is approximately 3 µm. The δ_x data, which are similar for δ_z, shows no measureable shear in the crack plane. The measurement distance excludes a region with low correlation coefficient (<0.3) close to the indentation; increasing the measurement distance up to 0.58 mm did not significantly affect the measured crack opening, showing that material displacements due to crack opening under the indentation load are measured consistently. The pattern of opening agrees with radial cracking of approximately 0.2 to 0.3 mm radius, under mode I loading from the indentation.

Discussion

It is common to present DVC data as effective strains (as in Figure 2), using the gradients of the displacement field to visualise deformations. Consequently the effects of non-corrected rigid body motions on the measured displacement field are not considered as such motions do not affect the strain field. The materials examined in this study have high elastic moduli and strength, and the indentation strain field is difficult to discriminate against a background that is influenced by noise in the displacement measurements. The calculated strain noise, estimated as the standard error from regions with negligible deformation remote from the indentations, was 0.52% for the Al-SiC composite and 0.23% for the Al_2O_3. After correcting for the small sample displacements and rotations that are inevitable in mechanical tests, the indentation displacement fields can be observed in the reference frame of the experiment, i.e. with the experimental vertical displacement parallel to the *z*-axis of the DVC data. Finite element simulation also provides displacements in the experiment reference frame, and so may be readily compared with data.

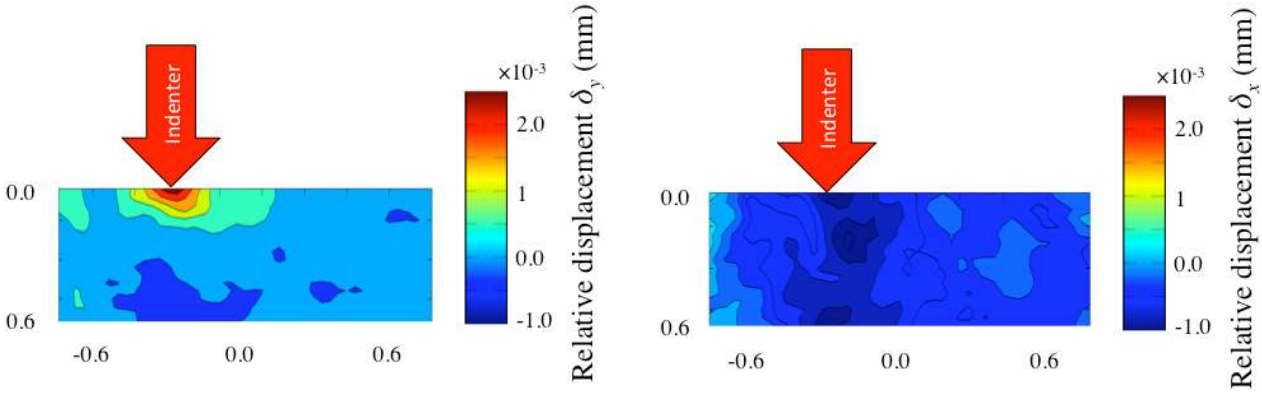

a) b)

Figure 7: Displacement difference fields across the Al_2O_3 indentation in the *xz* plane; a) δy and b) δx. (note, z=0 is 58 μm below the original surface). The indentation location is indicated by an arrow.

The agreement between the measured and predicted displacement fields in the Al-SiC composite demonstrates the effectiveness of DVC, even when applied to apparently poor quality tomographs. Due to the low attenuation contrast between the Al and SiC and with limited phase contrast, the microstructure of the Al-SiC is barely resolved, yet the random arrangement of fine SiC particles produces sufficient heterogeneous intensity for correlation to measure the relative displacements of microstructure regions. The disagreement between the measured and predicted displacements close to the indenter is significant. This may be due to large strains in this region, significantly changing the patterns of attenuation in the microstructure and so interfering with correlation. Such regions might be studied using a sequential of tomographic observations during indentation, or by displacement mapping via particle tracking [31] if higher contrast images with resolved microstructure features were obtainable.

The alumina analysis shows that displacements below the voxel resolution may be measured; radial cracking is confirmed by DVC and the opening profile and loading mode of a crack under an indentation are measured for the first time. The slight asymmetry observed in the crack opening displacements may be due to imperfections in the shape and alignment of the indenter.

Concluding Summary

This work has demonstrated that high resolution computed X-ray synchrotron tomography, analysed by DVC, can quantify the localised displacements associated with indentation testing in engineering materials. Plastic deformation in a ductile material has been measured and agrees with expectations; a more sophisticated FE simulation, for instance taking into account indenter/surface friction might achieve a better agreement [3]. In principle, material properties might be extracted by a reverse analysis of load-displacement response [1], with the simulated behaviour validated by measurements of the displacement field. The effects of temperature, ageing or irradiation damage in suitable microstructures might then be studied. In practice, the current data quality is insufficient as the displacements are not very sensitive to material properties. Nonetheless, this methodology may be useful for the interpretation of indentation deformation in more complex structures with gradients of material properties, such as strain-hardened surfaces and graded microstructures. Studies of localised plasticity at crack tips or notches in ductile materials are also feasible.

The analysis of brittle Al_2O_3 shows indentation induced radial cracking may be detected and quantified, even if it is not resolvable by tomographic imaging. A more detailed analysis of the Al_2O_3 data is in progress, including the effects of progressive loading and unloading to examine fracture toughness and residual stresses. In future, the progressive development of damage in materials such as brittle composites, with in-situ observations at elevated temperature, will be studied to better understand the relation between mechanical properties and microstructural damage.

Acknowledgements

This work was carried out with the support of the Diamond Light Source; the authors acknowledge the beam time award at the Joint Engineering, Environmental and Processing (I12) beamline (Experiment EE7119) and the help of Dr D.M. Collins, Dr H. Cetinel and Mr S. Barhli to conduct the experiment. MM and TJM gratefully acknowledge the support of Oxford Martin School and MM acknowledges the support of Linacre College, Oxford through a Junior Research Fellowship. The Manchester X-Ray Imaging Facility (Dr S.A. McDonald and Professor P.M. Mummery) are thanked for the loan of the loading rig. Professor R.I. Todd, The University of Oxford, is thanked for valuable discussions. Almath Crucibles, UK and AMC (Aerospace Metal Composites) are thanked for supplying the alumina and the high energy milled material for the Al-SiC composite.

References

[1] Beghini M, Bertini L, Fontanari V. Int. J. Solids Struct. 2006;43:2441.
[2] Giannakopoulos AE, Larsson PL, Vestergaard R. Int. J. Solids Struct. 1994;31:2679.
[3] Karthik V, Visweswaran P, Bhushan A, Pawaskar DN, Kasiviswanathan KV, Jayakumar T, Raj B. Int J Mech Sci 2012;54:7.
[4] Mesarovic SD, Fleck NA. Proc. R. Soc. A-Math. Phys. Eng. Sci. 1999;455:2707.
[5] Srikant G, Chollacoop N, Ramamurty U. Acta Mater. 2006;54:5171.
[6] Venkatesh TA, van Vleit KJ, Giannakopoulos AE, Suresh S. Scr Mater 2000;42:833.
[7] Busby JT, Hash MC, Was GS. J. Nucl. Mater. 2005;336:267.
[8] Deschamps A, Militzer M, Poole WJ. ISIJ Int 2001;41:196.
[9] Cook RF, Pharr GM. J Am Ceram Soc 1990;73:787.
[10] Ponton CB, Rawlings RD. Mater. Sci. Technol. 1989;5:865.
[11] Hild F, Roux S. Strain 2006;42:69.
[12] Duff J, Marrow TJ. Corrosion Sci 2012;68:34.
[13] Bay BK, Smith TS, Fyhire DP, Saad M. Exp. Mech. 1999;39:217.
[14] Mostafavi M, McDonald SA, Çetinel H, Mummery PM, Marrow TJ. Carbon 2013;59:325.
[15] Mostafavi M, McDonald SA, Mummery PM, Marrow TJ. Eng. Fract. Mech. 2013;In Press (http://dx.doi.org/10.1016/j.engfracmech.2012.11.023).
[16] Roux S, Hild F, Viot P, Bernard D. Compos Pt A-Appl Sci Manuf 2008;39:1253.
[17] Réthoré J, Limodin N, Buffière JY, Hild F, Ludwig W, Roux S. J. Strain Anal. Eng. Des. 2011;46:683.
[18] King A, Johnson G, Ludwig W, Marrow TJ. Science 2008;321:382.
[19] King A, Ludwig W, Herbig M, Buffiere JY, Khan AA, Stevens N, Marrow TJ. Acta Mater. 2011;59:6761.
[20] Marrow TJ, Buffiere JY, Withers PJ, Johnson G, Engelberg DL. Int. J. Fatigue 2004;26:717.
[21] Munch B, Trtik P, Marone F, Stampanoni M. Optics Expr. 2009;17:8567.
[22] http://physics.nist.gov/PhysRefData/Xcom/html/xcom1.html.
[23] Cloetens P, Pateyron-Salomé, Buffiere JY, Peix G, Baruchel J, Peyrin F, Schlenker M. J Appl Phys 1997;81:5878.
[24] Sheridan WT, Keller MR, O'Connor CM, Brooks RA, Hanson KM. Med Phys 1980;7:108.
[25] DaVis. User's Manual. Gottingen: LaVision GmbH,, 2012.
[26] Shoemaker K. Animating rotation with quaternion curves. In: Barsky BA, editor. Proceedings of SIGGRAPH '85, 19. San Fransisco, CA, USA, 1985.
[27] ABAQUS. User's Manual: Dassault Systèmes Simulia Corp., Providence, Rhode Island, Version 6.10, 2010.
[28] Knowles A. Development of aluminium matrix nanocomposites Department of Materials. Oxford: University of Oxford, 2011.
[29] Seo YH, Kang CG. Compos Sci Technol 1999;59:643.
[30] Marrow TJ, Luprano V, Roberts S. J Am Ceram Soc 1993;76:2915.
[31] Mueth DM, Debregeas GF, Karczmar GS, Eng PJ, Nagal SR, Jaeger HM. Nature 2000;406:358.